Magnetization of topological line-node semimetals

G. P. Mikitik and Yu. V. Sharlai
B. Verkin Institute for Low Temperature Physics and Engineering, Ukrainian Academy of Sciences, Kharkov 61103, Ukraine

(Received 22 November 2017; published 13 February 2018)

Using an approximate expression for the Landau levels of the electrons located near a nodal line of a topological line-node semimetal, we obtain formulas for the magnetization of this semimetal at an arbitrary shape of its line. It is also shown that the dependence of the chemical potential on the magnetic field can be strong in these materials, and this dependence can essentially influence the de Haas-van Alphen oscillations. The obtained results are applied to the rhombohedral graphite, which is one of the line-node semimetals. For this material, we find temperature and magnetic field dependencies of its magnetic susceptibility.

DOI: 10.1103/PhysRevB.97.085122

I. INTRODUCTION

In recent years, much attention has been given to the so-called topological semimetals [1–34]. In particular, it was predicted [5] that their magnetization exhibits unusual dependencies on the chemical potential ζ, the temperature T, and the magnetic field H. These dependencies can serve as a fingerprint of the topological semimetals, and appropriate experimental investigations can be useful in studying electron energy spectra of these materials.

There are several types of the topological semimetals. In the Weyl and Dirac semimetals, the electron energy bands contact at discrete points of the Brillouin zone and disperse linearly in all directions around these critical points. At present, a number of such semimetals were discovered [6–19]. The magnetization of these materials was theoretically analyzed in the papers [5,35–38]. One more type topological materials is the line-node semimetals in which the conduction and valence bands touch along lines in the Brillouin zone and disperse linearly in directions perpendicular to these lines. It is necessary to emphasize that the contact of the electron energy bands along the lines is the widespread phenomenon in crystals [25,39–41]. For example, such contacts of the bands occur in graphite [42], beryllium [43], aluminium [44], and $LaRhIn_5$ [45]. However, the degeneracy energy of the bands, ε_d, generally is not constant along such lines, and the ε_d varies between its minimum $\varepsilon_{\min}$ and maximum $\varepsilon_{\max}$ values, reaching them at certain points of the line. A crystal with the band-contact line can be named the topological semimetal if the difference $\varepsilon_{\max} - \varepsilon_{\min} \equiv 2\Delta$ is sufficiently small and if the chemical potential ζ of the electrons does not lie far away from the mean energy $\varepsilon_d^0 \equiv (\varepsilon_{\max} + \varepsilon_{\min})/2$ of the line. Various line-node semimetals were theoretically predicted and discovered experimentally in recent years [20–34]. The magnetic susceptibility of a crystal with a band-contact line characterized by large Δ was theoretically investigated many years ago [35,36]. It turned out that the susceptibility exhibits a giant anomaly when ζ approaches one of the energies $\varepsilon_{\min}$ or $\varepsilon_{\max}$, which correspond to the points of the electron topological transitions of $3\frac{1}{2}$ kind [40]. When one deals with the topological semimetals, the interval 2Δ is small, and the character of the anomaly in the susceptibility changes. The susceptibility in the case of the line-node semimetals was considered for weak magnetic fields in Ref. [46] and for arbitrary magnetic fields in Ref. [5]. However, in our paper [5], formulas for the magnetization were mainly obtained in the case of the semimetals with a closed band-contact line lying in a plane perpendicular to an axis of n-fold symmetry. Beside this, we did not consider the H dependence of the chemical potential ζ and the effect of this dependence on the magnetization. However, this dependence, as we shall see below, can be strong.

In this paper, we derive general formulas for the magnetization of a line-node semimetal with a band-contact line of an arbitrary shape, taking into account the dependence $\zeta(H)$. Then we apply these results to the case when the line terminates on opposite faces of the Brillouin zone. As an example of the semimetal in which this situation occurs, we consider the rhombohedral graphite [20,21,47,48].

II. ELECTRON SPECTRUM NEAR A BAND-CONTACT LINE

In the vicinity of a band-contact line along which the conduction and valance bands touch, let us introduce orthogonal curvilinear coordinates so that the axis "3" coincides with the line, Fig. 1. The axes "1" and "2" are perpendicular to the third axis at every point of the band-contact line, and the appropriate coordinates p_1 and p_2 are measured from this line. In these coordinates, near the line, the most general form of the electron spectrum for the conduction and valence bands looks like [40]

$$\varepsilon_{c,v} = \varepsilon_d(p_3) + \mathbf{a}_\perp \mathbf{p}_\perp \pm E_{c,v},$$
$$E_{c,v}^2 = b_{11} p_1^2 + b_{22} p_2^2, \qquad (1)$$

where $\varepsilon_d(p_3)$ describes a dependence of the degeneracy energy along the line [the $\varepsilon_{\max}$ and $\varepsilon_{\min}$ mentioned above are the maximum and minimum values of the function $\varepsilon_d(p_3)$]; $\mathbf{p}_\perp = (p_1, p_2, 0)$ and $\mathbf{a}_\perp = (a_1, a_2, 0)$ are the vectors perpendicular to the line; the parameters of the spectrum b_{11}, b_{22}, and $\mathbf{a}_\perp$ generally depend on p_3. It is implied here that the directions of the axes "1" and "2" are chosen so that the quadratic form $E_{c,v}^2$ is diagonal (these directions generally changes along the line). The vector $\mathbf{a}_\perp$ specifies the tilt of the Dirac spectrum in the p_1-p_2 plane. Below we shall consider only the case when the

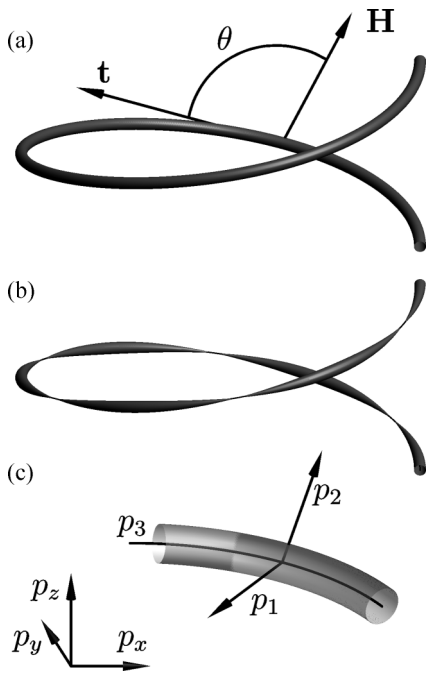

FIG. 1. The Fermi surface of the rhombohedral graphite as an example of the Fermi surface in a topological line-node semimetal at $|\zeta - \varepsilon_d^0| \gtrsim \Delta$ (a) and at $|\zeta - \varepsilon_d^0| < \Delta$ (b). The band-contact line lies inside the Fermi surface. The arrow shows the tangent vector $\mathbf{t}$ to the line at one of its points; θ is the angle between this $\mathbf{t}$ and the magnetic field $\mathbf{H}$. For clarity, we decrease the pitch of the helix. (c) A part of the Fermi surface, of the band-contact line and the two coordinate systems connected with the band-contact line (p_1-p_2-p_3) and with crystallographic axes of the rhombohedral graphite (p_x-p_y-p_z).

length of the vector $\tilde{\mathbf{a}}_\perp \equiv (a_1/\sqrt{b_{11}}, a_2/\sqrt{b_{22}}, 0)$ is less than unity [49],

$$\tilde{a}_\perp^2 = \frac{a_1^2}{b_{11}} + \frac{a_2^2}{b_{22}} < 1,$$

since at $\tilde{a}_\perp^2 > 1$ the magnetic susceptibility does not exhibit any essential anomaly in its dependencies on ζ, H, and T [5,35,36].

When the parameter $\Delta \equiv (\varepsilon_{\max} - \varepsilon_{\min})/2$ is small as compared to the characteristic scale of electron band structure (i.e., $\Delta \ll 1$ eV) and $\tilde{a}_\perp^2 < 1$, the Fermi surface $\varepsilon_{c,v}(\mathbf{p}_\perp, p_3) = \zeta$ of the semimetal looks like a narrow electron or hole tube for $\zeta - \varepsilon_d^0 \gtrsim \Delta$ or $\zeta - \varepsilon_d^0 \lesssim -\Delta$, respectively, Fig. 1. The band-contact line lies inside this tube. If $|\zeta - \varepsilon_d^0| < \Delta$, the Fermi surface has a self-intersecting shape and consists of the electron and hole pockets touching at some points of the line, i.e., it looks like "link sausages," Fig. 1. Thus, if the chemical potential ζ decreases and passes through the critical energies $\varepsilon_{\max} = \varepsilon_d^0 + \Delta$ and $\varepsilon_{\min} = \varepsilon_d^0 - \Delta$, the electron topological transitions occur [40]. At these transitions, the electron tube first transforms into the self-intersecting Fermi surface and then this surface transforms into the hole tube. We shall assume below that all transverse dimensions of the Fermi-surface tubes and pockets, which are of the order of $|\zeta - \varepsilon_d(p_3)|/V$, where $V \sim (b_{11}b_{22})^{1/4}$, are essentially less than the characteristic radius of curvature for the band-contact line. In this case, practically all electron orbits in the Brillouin zone, which are intersections of the Fermi surface with planes perpendicular to the magnetic field, are small and lie near the band-contact line. In other words, a small region in the Brillouin zone determines the local electron energy spectrum in the magnetic field almost for any point of the line. This spectrum has the form (see Appendix)

$$\varepsilon_{c,v}^l(p_3) = \varepsilon_d(p_3) \pm \left(\frac{e\hbar\alpha H|\cos\theta|}{c} l\right)^{1/2}, \quad (2)$$

$$\alpha = \alpha(p_3) = 2(b_{11}b_{22})^{1/2}(1 - \tilde{a}_\perp^2)^{3/2}, \quad (3)$$

where l is a non-negative integer ($l = 0, 1, ...$), with the single Landau subband $l = 0$ being shared between the branches "c" and "v," and $\theta = \theta(p_3)$ is the angle between the direction of the magnetic field and the tangent $\mathbf{t} = \mathbf{t}(p_3)$ to the band-contact line at the point with a coordinate p_3, Fig. 1. Formula (2) fails only for those points of the line for which θ is close to $\pi/2$. However, these points do not give a noticeable contribution to the magnetization [35].

III. MAGNETIZATION

We define the vector of the magnetization as $-\partial\Omega/\partial H_i$, where Ω is the Ω potential per unit volume of a crystal, and we disregard a contribution to the magnetization associated with the electron *surface* states of a topological semimetal. When the chemical potential ζ does not lie far away from ε_d^0, the total magnetization consists of its special part M_i determined by the electron states located near the band-contact line and a background term $\chi_{ij}^0 H_j$ in which the practically constant tensor χ_{ij}^0 is specified by electron states located far away from this line,

$$M_i^{\text{total}} = M_i + \chi_{ij}^0 H_j.$$

It is the special part M_i that is responsible for dependencies of the magnetization on the chemical potential, temperature, and for a nonlinear dependence of the magnetization on the magnetic field magnitude. It is also significant that $|M_i|$ is not small as compared to $|\chi_{ij}^0 H_j|$ and can essentially exceed this background term for the topological semimetals [5]. Below we calculate M_i only.

In weak magnetic fields $H \ll H_T$, when the characteristic spacing $\Delta\varepsilon_H$ between the Landau subbands is much less than the temperature T, the magnetization M_i is proportional to H. On the other hand, at $H > H_T$, when $\Delta\varepsilon_H > T$, the magnetization becomes a nonlinear function of H. The background term χ_{ij}^0 in the susceptibility remains constant at all magnetic fields. According to Eq. (2), we have the following estimate for the spacing $\Delta\varepsilon_H$ between the Landau subbands of electrons in the magnetic field: $\Delta\varepsilon_H \sim (e\hbar H V^2/c)^{1/2}$, and hence

$$H_T \sim \frac{cT^2}{e\hbar V^2}.$$

If the characteristic velocity $V \approx (b_{11}b_{22})^{1/4} \sim 10^6$–$10^5$ m/s, one obtains $H_T \sim$ 2–200 Oe at $T = 4$ K [50]. In other words, for the topological semimetals investigated at low temperatures, a nonlinear dependence of M_i^{total} on H can develop at sufficiently low magnetic fields.

Using formulas (2) and (3), the special part of the magnetization associated with the band-contact line can be calculated at magnetic fields of an arbitrary strength. In such calculations,

we shall suppose that Eqs. (2) and (3) are valid at all angles θ including $\theta = \pi/2$. As was mentioned above [see also Eq. (15)], this supposition does not introduce essential errors into the results. As is clear from formula (2), within this approximation, a contribution of electron states located near a point p_3 to the special part of the Ω potential is determined only by the magnetic field component $H\cos[\theta(p_3)]$ parallel to the appropriate tangent $\mathbf{t}(p_3)$ to the line, and hence the magnetization of these states is parallel to this tangent, too. Eventually, we obtain the following expressions for the Ω potential and the magnetization at $T = 0$ [51]:

$$\Omega(\zeta,H) = -\frac{e^{3/2}H^{3/2}}{2\pi^2\hbar^{3/2}c^{3/2}}\int_0^L dp_3|\cos\theta|^{3/2}\sqrt{\alpha(p_3)}K_1(u), \tag{4}$$

$$\mathbf{M}(\zeta,H) = \frac{e^{3/2}H^{1/2}}{2\pi^2\hbar^{3/2}c^{3/2}}\int_0^L dp_3|\cos\theta|^{1/2}\nu\sqrt{\alpha(p_3)}K(u)\mathbf{t}, \tag{5}$$

where the integration in the Brillouin zone is carried out over the band-contact line of the length L; $\theta = \theta(p_3)$ is angle between $\mathbf{t} = \mathbf{t}(p_3)$ and $\mathbf{H}$; $\nu = \nu(p_3)$ is a sign of $\cos\theta$;

$$K_1(u) = \zeta\left(-\tfrac{1}{2},[u]+1\right) + \sqrt{u}\left([u]+\tfrac{1}{2}\right) - \tfrac{1}{3}u^{3/2}, \tag{6}$$

$$K(u) = \tfrac{3}{2}\zeta\left(-\tfrac{1}{2},[u]+1\right) + \sqrt{u}\left([u]+\tfrac{1}{2}\right), \tag{7}$$

$\zeta(s,a)$ is the Hurwitz zeta function,

$$u = \frac{[\zeta-\varepsilon_d(p_3)]^2c}{e\hbar\alpha(p_3)H|\cos\theta|} = \frac{cS(p_3)}{2\pi e\hbar H}, \tag{8}$$

$S(p_3)$ is the area of the Fermi-surface cross section by the plane perpendicular to the magnetic field and passing through the point with the coordinate p_3, and $[u]$ is the integer part of u ($[u]$ is the number of the Landau levels lying below ζ at the point p_3). In deriving Eqs. (4) and (5), we have assumed the twofold degeneracy of the electron bands in spin. In absence of this degeneracy (for a noncentrosymmetric semimetal with a strong spin-orbit interaction), the right-hand sides of formulas (4) and (5) should be divided by two. In the case of a closed band-contact line, formula (5) reproduces Eqs. (44), (46), and (47) of Ref. [5]. For nonzero T, the Ω potential and the magnetization $M_i(\zeta,H,T)$ can be calculated with the relationships [52]:

$$\Omega(\zeta,H,T) = -\int_{-\infty}^{\infty}d\varepsilon\Omega(\varepsilon,H,0)f'(\varepsilon), \tag{9}$$

$$M_i(\zeta,H,T) = -\int_{-\infty}^{\infty}d\varepsilon M_i(\varepsilon,H,0)f'(\varepsilon), \tag{10}$$

where $f'(\varepsilon)$ is the derivative of the Fermi function,

$$f'(\varepsilon) = -\left[4T\cosh^2\left(\frac{\varepsilon-\zeta}{2T}\right)\right]^{-1}. \tag{11}$$

In the topological semimetals, charge carriers (electron and holes) are located near the band-contact line, and their chemical potential ζ generally depends on the magnetic field, $\zeta = \zeta(H)$. This dependence can be derived from the condition that the charge carrier density n does not vary with increasing H,

$$n(\zeta,H) = n_0(\zeta_0), \tag{12}$$

where n_0 and ζ_0 are the density and the chemical potential at $H = 0$,

$$n(\zeta,H) = n_0(\zeta) - \frac{\partial\Omega}{\partial\zeta},$$

and Ω is given by Eq. (4). With Eqs. (1), (2), and (4), one finds the following expressions for $n_0(\zeta_0)$ and $n(\zeta,H)$ at $T = 0$:

$$n_0(\zeta_0) = \frac{1}{2\pi^2\hbar^3}\int_0^L dp_3\frac{(\zeta_0-\varepsilon_d(p_3))^2\sigma(\zeta_0-\varepsilon_d(p_3))}{\alpha(p_3)}, \tag{13}$$

$$n(\zeta) = \frac{eH}{2\pi^2c\hbar^2}\int_0^L dp_3|\cos\theta|\sigma(\zeta-\varepsilon_d(p_3))\left(\frac{1}{2}+[u]\right), \tag{14}$$

where $\sigma(x) = 1$ if $x > 0$, and -1 otherwise. The other notations are the same as in formulas (4)–(8). At nonzero temperatures, $n_0(\zeta_0,T)$ and $n(\zeta,H,T)$ can be calculated with formulas similar to Eq. (9). On calculating $\zeta(H)$ with Eqs. (12)–(14), one can find the magnetization as a function of n_0 or ζ_0, inserting $\zeta(H)$ into Eq. (5).

Consider now several limiting cases. In the weak magnetic field, $H \ll H_T$, the Ω potential described by formulas (4) and (9) becomes proportional to H^2 [51]. Eventually, we arrive at linear dependence of the magnetization on the magnetic field,

$$\mathbf{M}(\zeta,H,T) = \frac{e^2H}{12\pi^2\hbar c^2}\int_0^L dp_3\alpha(p_3)f'(\varepsilon_d)\cos\theta\,\mathbf{t}. \tag{15}$$

This formula agrees with Eq. (35) of Ref. [5]. Note also that points of the band-contact line for which θ is close to $\pi/2$ give a small contribution to the magnetization. Equation (15) leads to the following expression for the magnetization component $M_\parallel$ parallel to the magnetic field:

$$M_\parallel(\zeta,H,T) = \frac{e^2H}{12\pi^2\hbar c^2}\int_0^L dp_3\alpha(p_3)f'(\varepsilon_d)\cos^2\theta.$$

Interestingly, this expression can be easily understood from the following considerations: at a given p_3, the Landau levels described by Eq. (2) look like the levels of electrons near the Dirac point of graphene, $\varepsilon_l = \pm(2e\hbar V_D^2Hl/c)^{1/2}$, if the energy of the Dirac point coincides with $\varepsilon_d(p_3)$, and the electron velocity V_D at this point is given by $V_D^2 = \alpha|\cos\theta|/2$. In the weak magnetic field H perpendicular to the "graphene" plane, the electron magnetic moment of the Dirac point has the form [53]:

$$\frac{e^2V_D^2H}{3\pi c^2}f'(\varepsilon_d) = \frac{e^2\alpha|\cos\theta|H}{6\pi c^2}f'(\varepsilon_d).$$

Multiplying this expression by $dp_3|\cos\theta|/2\pi\hbar$ (the number of the "graphene" planes in the interval dp_3) and integrating over the band-contact line, we arrive at the above formula for $M_\parallel$.

In strong magnetic fields, $T \ll \Delta\varepsilon_H$, and if $|\zeta-\varepsilon_{\min}|$, $|\zeta-\varepsilon_{\max}| \ll \Delta\varepsilon_H$, the argument u in $K(u)$ is small practically for all points of the band-contact line, and hence $K(u) \approx$

$(3/2)\zeta(-1/2,1) \approx -0.98/\pi$. In this case, formula (5) gives $M_i \propto H^{1/2}$ with a proportionality coefficient depending on the direction of the magnetic field and the shape of the band-contact line. In particular, we find the following expression for longitudinal component of the magnetization:

$$M_{\parallel}(H) = \frac{3\zeta(-1/2,1)e^{3/2}H^{1/2}}{4\pi^2\hbar^{3/2}c^{3/2}} \int_0^L dp_3 |\cos\theta|^{3/2}\sqrt{\alpha(p_3)}.$$

As in the case of weak magnetic fields, this formula can be represented in the form: $\int_0^L dp_3|\cos\theta|M_D/2\pi\hbar$, where M_D is the electron magnetic moment of the Dirac point in strong magnetic fields [54],

$$M_D = \frac{3\zeta(-1/2,1)e^{3/2}V_D H^{1/2}}{\sqrt{2}\pi\hbar^{1/2}c^{3/2}} = \frac{3\zeta(-1/2,1)e^{3/2}(\alpha|\cos\theta|H)^{1/2}}{2\pi\hbar^{1/2}c^{3/2}}.$$

As to condition (12), in strong magnetic fields and at low temperatures, it leads to a shift of the chemical potential into the interval: $\varepsilon_{\min} < \zeta < \varepsilon_{\max}$.

In the region of the magnetic fields when $T \ll \Delta\varepsilon_H \ll |\zeta - \varepsilon_{\min}|, |\zeta - \varepsilon_{\max}|, 2\Delta$, it follows from Eq. (5) [51] that the magnetization is described by the usual formula [55] for the de Haas-van Alphen effect, with the phase of the oscillations being shifted by π [56]. This shift is the characteristic feature of crystals with a band-contact line and is due to the Berry phase π for the electron orbits surrounding this line [56,57]. In the equivalent interpretation [58,59] allowing a nonzero spin-orbit coupling, this shift is caused by the large value of the orbital g factor, $g = 2m/m_*$, occurring even at a weak spin-orbit interaction. Here, m_* is the cyclotron mass and m is the electron mass. As in usual metals [55], the dependence $\zeta(H)$ is sufficiently weak in this region of the magnetic fields and practically has no effect on the oscillations.

At small Δ when $T < 2\Delta \ll \Delta\varepsilon_H \ll |\zeta - \varepsilon_{\min}|$, $|\zeta - \varepsilon_{\max}|$, the spectrum (2) transforms, in fact, into the spectrum of a two-dimensional electron system since different Landau subbands $\varepsilon^l_{c,v}(p_3)$ do not overlap, and they look like broadened Landau levels. In this case, when H changes, the chemical potential $\zeta(H)$ moves together with one of these levels, and then, at a certain value of H, it jumps from this level to the neighboring one [55], Fig. 2. This strong dependence $\zeta(H)$ noticeably changes the shape of the de Haas-van Alphen oscillations (see the next section) and can mask the correct value of the Berry phase when it is measured with these oscillations. Indeed, the jumps occur at the fields H_l for which $n(\zeta)$ in Eq. (14) becomes independent of ζ. This situation is realized when $[u]$ in the right hand side of Eq. (14) is one and the same integer l along the whole line. Then, Eq. (12) takes the form

$$\frac{1}{H_l} = \frac{eC}{2\pi^2 c\hbar^2}\left(l + \frac{1}{2}\right),$$

where the constant C is the ratio of $\int_0^L dp_3|\cos\theta|$ to $n_0(\zeta_0)$. It follows from this equation that the dependence of $1/H_l$ on l is a straight line that intersects the l axis at $l = -1/2$, i.e., the Landau-level fan diagram plotted with the fields H_l looks like in the case when the Berry phase Φ_B is equal to zero [55,56]. If $\Delta\varepsilon_H$ (i.e., H) decreases and becomes comparable with 2Δ,

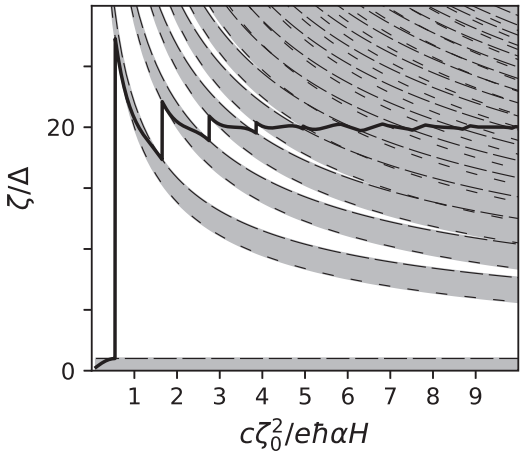

FIG. 2. The dependence of chemical potential ζ (measured from ε_d^0) on $1/H$ calculated with Eqs. (12)–(14) at $\zeta(H=0) \equiv \zeta_0 = 20\Delta$, $\varepsilon_d(p_3) = \Delta\cos(2\pi p_3/L)$, $\cos\theta = 1$, and $\alpha(p_3) = \text{const}$. We also mark the Landau subbands, Eq. (2), by the dark background, and the short and long dashes indicate the lower and the upper edges of these subbands, respectively. The crossover described in the text occurs at $c\zeta_0^2/e\hbar\alpha H \sim 5$.

a crossover from the quasi-two-dimensional electron spectrum to the three-dimensional one occurs, the jumps in ζ smooth, and the appropriate Landau-level fan diagram can give an intermediate value of the "Berry phase" lying between 0 and π.

Strictly speaking, the quasi-two-dimensional electron spectrum in magnetic fields does not appear in every topological semimetal with a small Δ since if $\cos\theta \to 0$ in some part of the line, the $\Delta\varepsilon_H$ becomes less than 2Δ there [see Eq. (2)]. For the quasi-two-dimensional spectrum to occur, a change of the quantity $u \propto 1/\cos\theta$ along the line should be less than unity, i.e., $1/\cos\theta$ may change only within a sufficiently small interval. This imposes a restriction on the shape of the nodal line. It is clear that the spectrum of this kind can appear for a straight band-contact line, i.e., for a symmetry axis, since $\theta(p_3)$ is constant in this case. As will be shown in the next section, the quasi-two-dimensional spectrum is also possible in the case of band-contact lines terminating on the opposite faces of the Brillouin zone for a certain region of the magnetic-field directions. This type of the spectrum can also occur for a closed band-contact line composed of nearly straight arcs. This situation appears to take place in ZrSiS [29,30]. Besides, the spectra including the quasi-two dimensional and three-dimensional parts can appear in the line-node semimetals containing several small groups of charge carriers. In this case, one may expect to find a noticeable dependence of ζ on H and to obtain the intermediate values of Φ_B in the measurements of the de Haas-van Alphen oscillations.

Using various oscillation effects observed in magnetic fields, the Berry phase was recently found in the experiments with ZrSiS [60–65] and with ZrSiTe or ZrSiSe [66], and the intermediate values of this phase (other than 0 and π) were obtained for a number of the electron orbits. Taking into account the above considerations, one may hypothesize that the essential dependence of chemical potential on the magnetic field takes place in these experiments. This dependence is

probably associated with the existence of an electron group for which the quasi-two-dimensional spectrum or the crossover to this spectrum occurs in the magnetic-field range under study in these semimetals.

For comparison, let us discuss the well-known measurements of the Berry phase in graphene [67,68]. These measurements revealed the genuine Berry phase π for the electron orbits surrounding the Dirac point, even though one might expect a strong dependence of the chemical potential on H in this two-dimensional material. However, the oscillation experiments described in Refs. [67,68] were carried out at fixed values of the gate voltage. This means that the measurements were made at constant chemical potential rather than at constant number of the charge carriers, and so the true value of the Berry phase was found in these experiments.

Finally, it is worth noting that the obtained results for the magnetization can be useful in describing the magnetostriction of the topological semimetals [69].

IV. RHOMBOHEDRAL GRAPHITE

We now apply the above results to the rhombohedral graphite [20,21,47,48]. According to Ref. [48], in this material there is a band-contact line that has the shape of a helix terminating on the opposite faces of the Brillouin zone, Fig. 1. In the simplest model of Ref. [48], the helix is described as follows:

$$p_x = p_0 \cos\phi, \quad p_y = p_0 \sin\phi, \quad p_z = \frac{\hbar}{d}\Big(\phi - \frac{\pi}{6}\Big), \tag{16}$$

where the p_x-p_y plane of the quasimomentum space coincides with the basal plane of the crystal, and the third component of the quasimomentum, p_z, is perpendicular to this plane; ϕ is the angle defining the direction of the quasimomentum in the p_x-p_y plane; $d \approx 3.35$ Å is the interlayer distance in the rhombohedral graphite, and $p_0 = \gamma_1/v_F$ is a constant, with $\gamma_1 \approx 0.39$ eV, $v_F = 1.5\gamma_0 a_0/\hbar \approx 1.04 \times 10^6$ m/sec, $a_0 = 1.42$ Å, and $\gamma_0 = 3.2$ eV being the parameters of the model. Within this model, the electron spectrum near the helicoidal band-contact line reduces to Eq. (1) with $\varepsilon_d(p_3) = 0$ (from here on, we measure electron energies from the energy of the band degeneracy), $\mathbf{a}_\perp = 0$, and

$$\begin{aligned} b_{11} &= v_F^2, \\ b_{22} &= v_F^2\big(1 + \tilde{p}_0^2\big), \\ \alpha(p_3) &= 2v_F^2\sqrt{1 + \tilde{p}_0^2}, \end{aligned} \tag{17}$$

where $\tilde{p}_0 \equiv p_0 d/\hbar \approx 0.19$. Thus, in the model, b_{11}, b_{22} and $\alpha(p_3)$ are constant along the line, and the parameter $\Delta \equiv \varepsilon_{\max} - \varepsilon_{\min} = 0$. With formulas (16), one can find the tangent vector $\mathbf{t}$ to the line,

$$\mathbf{t} = \frac{1}{\sqrt{1 + \tilde{p}_0^2}}(-\tilde{p}_0 \sin\phi, \tilde{p}_0 \cos\phi, 1), \tag{18}$$

and the infinitesimal element dp_3,

$$dp_3 = \frac{\hbar\sqrt{1 + \tilde{p}_0^2}}{d} d\phi, \tag{19}$$

which are both expressed in terms of the angle ϕ.

Let the magnetic field $\mathbf{H}$ have the components

$$\mathbf{H} = H(\sin\theta_H \cos\phi_H, \sin\theta_H \sin\phi_H, \cos\theta_H),$$

where the angles θ_H and ϕ_H define its direction relative to the crystal axes x, y, and z. Then, a simple calculation gives

$$\cos\theta = \frac{1}{\sqrt{1 + \tilde{p}_0^2}}\lambda(\theta_H, \varphi), \tag{20}$$

$$u = \frac{\zeta^2 c}{2e\hbar v_F^2 |\lambda(\theta_H, \varphi)| H}, \tag{21}$$

where $\varphi = \phi - \phi_H$,

$$\lambda(\theta_H, \varphi) = \cos\theta_H - \tilde{p}_0 \sin\theta_H \sin\varphi. \tag{22}$$

With Eqs. (17)–(22) and (5), we obtain the following expressions for the magnetization components at $T = 0$:

$$\mathbf{M}_{xy} = -\frac{\tilde{p}_0 v_F H^{1/2}}{\sqrt{2}\pi^2 d}\Big(\frac{e}{\hbar c}\Big)^{3/2} \mathbf{h}_\perp \int_{-\pi}^{\pi} d\varphi \sin\varphi |\lambda|^{1/2} \nu_\lambda K(u), \tag{23}$$

$$M_z = \frac{v_F H^{1/2}}{\sqrt{2}\pi^2 d}\Big(\frac{e}{\hbar c}\Big)^{3/2} \int_{-\pi}^{\pi} d\varphi |\lambda|^{1/2} \nu_\lambda K(u), \tag{24}$$

where $\lambda = \lambda(\theta_H, \varphi)$, ν_λ is the sign of λ, the direction of the component M_{xy} in the x-y plane is determined by the unit vector $\mathbf{h}_\perp = (\cos\phi_H, \sin\phi_H, 0)$, u is given by Eq. (21). With Eqs. (23) and (24), one can also calculate the magnetic torque $K = H(M_z \sin\theta_H - M_{xy} \cos\theta_H)$. For weak magnetic fields, Eq. (15) yields

$$\mathbf{M} = \frac{e^2 v_F^2 H}{6\pi c^2 d} f'(0)\big(\tilde{p}_0^2 \sin\theta_H \mathbf{h}_\perp + 2\cos\theta_H \mathbf{z}\big), \tag{25}$$

where $\mathbf{z}$ is the unit vector along z axis. Since $\tilde{p}_0^2 \approx 0.04$, this formula shows that at $\frac{\pi}{2} - \theta_H \gg 0.02$, the magnetization is mainly directed along z axis, and $|M_z/H_z|$ can reach a large value of the order of $0.016/T$ where T is measured in Kelvin.

The background susceptibility tensor χ_{ij}^0 for rhombohedral graphite has the two components: χ_{zz}^0 and $\chi_{xx}^0 = \chi_{yy}^0 = \chi_\perp^0$, and hence the total magnetization $\mathbf{M}^{\text{total}}$ is described by the formulas

$$\begin{aligned} M_z^{\text{total}} &= M_z + \chi_{zz}^0 H \cos\theta_H, \\ M_{xy}^{\text{total}} &= \mathbf{M}_{xy} + \chi_\perp^0 H \sin\theta_H \mathbf{h}_\perp. \end{aligned}$$

The constants χ_{zz}^0 and $\chi_\perp^0$ are independent of the temperature, chemical potential and magnetic field, and so the background terms have no effect on dependences of the total magnetic susceptibility on H, ζ, and T. But it is well to bear in mind that these terms can be generally essential in analyzing experimental θ_H-dependencies of M_z^{total} and M_{xy}^{total}.

Consider the case of the "ideal" semimetal (without any doping) when $\zeta = 0$. In this situation, it follows from formulas (10), (23), and (24) that for any component M_i of the magnetization, the combination TM_i/H depends only on the direction of the magnetic field and on the ratio H/T^2, i.e., on H/H_T where we define H_T from the condition

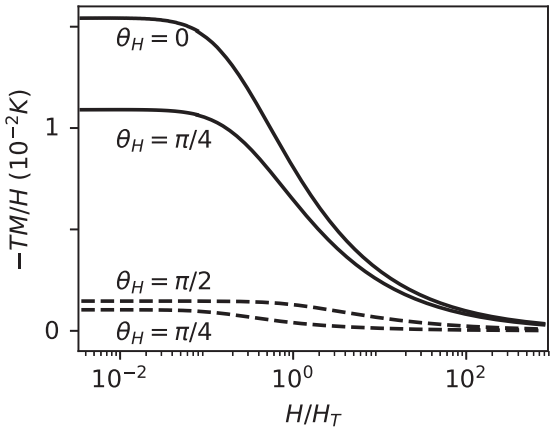

FIG. 3. Dependencies of TM_z/H (solid lines) and of $TM_{xy}/(\tilde{p}_0 H)$ (dashed lines) on H/H_T calculated numerically with Eqs. (10), (23), and (24) at $\zeta = 0$ and $\theta_H = 0, \pi/4$ for M_z and $\theta_H = \pi/2, \pi/4$ for M_{xy}. The H_T is given by Eq. (26). At $H/H_T \gg 1$, the combinations $TM_z(H)/H$ and $TM_{xy}(H)/H$ are proportional to $(H_T/H)^{1/2}$.

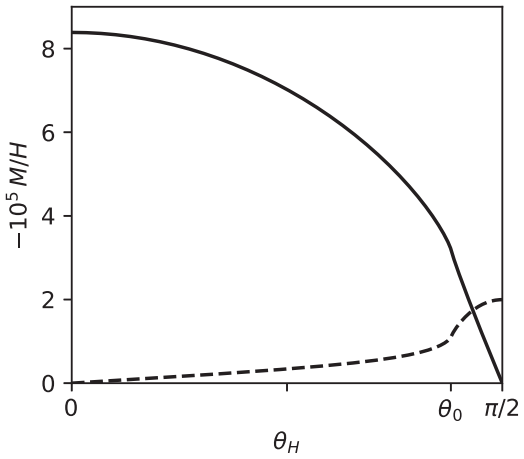

FIG. 4. Dependencies of M_z/H (the solid line) and of $M_{xy}/(\tilde{p}_0 H)$ (the dashed line) on the tilt angle θ_H of the magnetic field $H = 10$ T. The dependencies are calculated numerically with Eqs. (10), (23), and (24) at the temperature 4.2 K and $\zeta = 0$. The angle θ_0 is defined by Eq. (27). With decreasing H, the dependencies remain qualitatively unchanged, but values of $M_z(0)/H$ and $M_{xy}(\pi/2)/H$ increase in agreement with Fig. 3.

$$|\varepsilon^1_{c,v} - \varepsilon^0_{c,v}|_{\theta=0} = T,$$

$$H_T = \frac{cT^2}{2e\hbar v_F^2\sqrt{1+\tilde{p}_0^2}}. \tag{26}$$

In Fig. 3, we show the H dependencies of the combinations TM_z/H and $TM_{xy}/(\tilde{p}_0 H)$ for $\theta_H = 0, \pi/4$, and $\theta_H = \pi/4, \pi/2$, respectively. It is seen that at weak fields $H \ll H_T$, the magnitude of the magnetic susceptibility $|M_i/H|$ is maximum and is proportional to $1/T$ in agreement with Eq. (25). For strong magnetic fields $H \gg H_T$, we find that $TM_i/H \propto (H_T/H)^{1/2}$, i.e., $M_i \propto H^{1/2}$ in accord with the result of the previous section. At fixes H and T, the angular dependencies of M_z and M_{xy} are shown in Fig. 4. The component M_z is zero when the magnetic field lies in the x-y plane, whereas M_{xy} vanishes at $\theta_H = 0$. The characteristic angle θ_0 visible as a crossover point in the plot is determined by the equality,

$$\cot\theta_0 = \tilde{p}_0. \tag{27}$$

The origin of this crossover is the following. At $\theta_H > \theta_0$, points in the band-contact line exist for which the tangent to the line is perpendicular to the magnetic field, whereas for $\theta_H < \theta_0$, such points are absent. In our approximation, these points do not give any contribution to the magnetization, and the appearance of these points at $\theta_H > \theta_0$ leads to the crossover.

Of course, for real samples of the rhombohedral graphite, one cannot expect that the doping is completely absent, and $\zeta = 0$. Besides, as was mentioned in Introduction, the parameter Δ always differs from zero in the line-node semimetals. A more accurate model of Ref. [48] for electron energy spectrum of the rhombohedral graphite shows that ε_d has the form:

$$\varepsilon_d \approx -\Delta\cos(3p_z d/\hbar) = -\Delta\sin 3\phi, \tag{28}$$

where $\Delta \approx 2\gamma_4\gamma_3\gamma_1/\gamma_0^2 \approx 1$ meV, $\gamma_4 = 44$ meV, and $\gamma_3 \approx 315$ meV. The data of Figs. 3 and 4 will remain unchanged if ζ and Δ do not exceed T or $\Delta\varepsilon_H$, i.e., if $\Delta, \zeta \ll \max(T, \Delta\varepsilon_H)$ where $\Delta\varepsilon_H[\text{meV}] \sim 0.4\sqrt{H[\text{Oe}]}$. In Fig. 5, we present the H dependence of M_z/H when at least ζ does not satisfy this restriction. The de Haas-van Alphen oscillations are clearly visible in the figure. The dashed line shows the oscillations calculated at constant ζ. Since the phase of these oscillations is determined by the Berry phase Φ_B for the appropriate electron orbits [56], this Φ_B can be found with the Landau-level fan diagram shown in the upper inset of Fig. 5. (As expected, this inset yields $\Phi_B = \pi$.) However, $\Delta\varepsilon_H$ at the Fermi level exceeds 2Δ for $H > H_{\text{cr}}$, where $H_{\text{cr}} \sim 4\Delta\zeta c/e\hbar\alpha \sim 2$ kOe is the crossover field separating the regions of the quasi-two-dimensional and three-dimensional regimes of the oscillations. In other words, for the whole interval of the magnetic fields presented in Fig. 5, the electron spectrum is quasi-two-dimensional, and one has $\delta u < 1$ for such magnetic fields. Here $\delta u \approx (4\Delta/\zeta)u$ is the variation of u along the band-contact line. Then, as explained in the previous section, the chemical potential exhibits jumps when the middle of the interval between the appropriate Landau subbands crosses ζ_0, the chemical potential at zero magnetic field, Fig. 5. At these H, the magnetization M_z experiences jumps, too, and the positions of these jumps do not coincide with the sharp peaks of M_z/H calculated at a constant chemical potential. In other words, there is a shift of the oscillations associated with the dependence $\zeta(H)$, and this shift imitates a change of the Berry phase Φ_B. In particular, the lower inset in Fig. 5 suggest that $\Phi_B = 0$ although the Berry phase is still equal to π for the electron orbits in the magnetic fields. Note also that when the dependence $\zeta(H)$ is taken into account, the shape of the oscillations essentially changes as compared to the shape of the oscillations calculated at $\zeta = \text{const}$.

If the magnetic field is tilted away from the z axis, the $\cos\theta$ is no longer constant along the line, and the crossover from the three-dimensional electron spectrum to the quasi-two-dimensional one develops at the higher magnetic fields than 2 kOe. For the quasi-two-dimensional spectrum to occur, it is necessary that $(\delta\cos\theta/\cos\theta)u < 1$ where $\delta\cos\theta$ is the variation of $\cos\theta$ along the line. Using Eqs. (20)–(22), we obtain

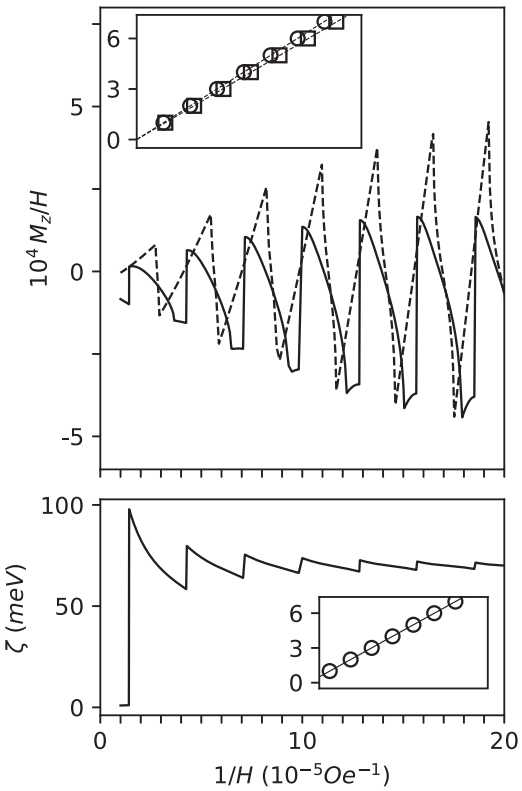

FIG. 5. (Top) Dependencies of M_z/H on H at $T = 0$ and the magnetic field directed along z axis. The dependencies are calculated numerically with Eqs. (5), (7), (8), (17)–(20), (22), and (28). The dashed line corresponds to the constant chemical potential $\zeta = 70$ meV, the solid line shows M_z/H at $\zeta_0 = 70$ meV, taking into account the H-dependence of ζ presented in the bottom panel. The inset: the Landau-level fan diagram plotted with the positions of the maxima (circles) and the minima (squares) of the dashed curve in the main top panel. (Bottom) The H dependence of the chemical potential calculated with Eqs. (12)–(14) at $\zeta_0 = 70$ meV. The inset shows the Landau-level fan diagram plotted with the positions of the maxima of the solid curve in the top panel.

$(\delta \cos\theta/\cos\theta) \approx 2\tilde{p}_0 \tan\theta_H$ and apart from $(4\Delta/\zeta)u < 1$, the additional condition on H: $c\zeta^2\tilde{p}_0 \tan\theta_H/(e\hbar V_F^2 \cos\theta_H) < H$. At $\zeta = 70$ meV, this condition has no effect on the crossover field $H_{cr} \sim 2$ kOe when $\theta_H \lesssim 10^\circ$. However, at $\theta_H > 10^\circ$, the crossover magnetic field is determined by this additional condition and increases due to the factor $\tan\theta_H/\cos\theta_H$.

Interestingly, some results of Figs. 4 and 5 can be semiquantitatively understood if we formally set $\tilde{p}_0 \ll 1$ in the above formulas. In this case the band-contact helix will look like a practically straight line terminating on the opposite faces of the Brillouin zone, λ in Eq. (22) tends to $\cos\theta_H$, M_{xy} defined by Eq. (23) becomes small, and Eqs. (23) and (24) at $\cot\theta_H \gg \tilde{p}_0$ transform into

$$M_z \approx \frac{v_F(2H|\cos\theta_H|)^{1/2}}{\sqrt{\pi}d}\left(\frac{e}{\hbar c}\right)^{3/2} \nu_H K(u),$$

$$\mathbf{M}_{xy} \approx \frac{\tilde{p}_0^2}{4}\tan\theta_H \mathbf{h}_\perp M_z, \tag{29}$$

where ν_H is a sign of $\cos\theta_H$, and u is given by Eq. (21) with $\lambda = \cos\theta_H$. At small u, one has $K(u) \approx$ const, and M_z is proportional to $|\cos\theta_H|^{1/2}$, whereas $M_{xy} \propto \sin\theta_H/|\cos\theta_H|^{1/2}$; cf. Fig. 4. Since at $u \gg 1$, $K(u)$ is the oscillating function of u,

$$K(u) \approx 0.5\sqrt{u}(u - [u] - 0.5), \tag{30}$$

Eqs. (29) shows that M_z and M_{xy} oscillate with changing $H|\cos\theta_H|$, cf. Fig. 5.

V. CONCLUSIONS

Whatever the shape of the band-contact line in a topological line-node semimetal, formulas (5), (7), (8), and (10)–(15) enable one to calculate the magnetization of this semimetal either as a function of chemical potential or as a function of the charge-carrier density in it. The formulas take into account a dispersion of the degeneracy energy ε_d along the nodal line, but it is implied in their deriving that the difference $\varepsilon_{max} - \varepsilon_{min} \equiv 2\Delta$ between the maximal and minimal values of ε_d is essentially less than the characteristic scale ($\sim$1 eV) of the electron-band structure of crystals. In the case of the semimetal with a closed band-contact line lying in a plane perpendicular to an axis of n-fold symmetry, the obtained formulas reduce to those derived in Ref. [5].

At low temperatures the magnetization of the line-node semimetals generally exhibits the de Haas-van Alphen oscillations, and these oscillations are shifted in phase as compared to the case of usual metals due to the Berry phase π for electron orbits surrounding the band-contact line. This shift is the characteristic property of the topological line-node semimetals. However, the H dependence of the chemical potential can be strong in these semimetals, and the shift of the oscillations can differ from π, simulating the case of the Berry phase deviating from this value.

To illustrate the obtained formulas, we apply them to rhombohedral graphite and calculate dependencies of the magnetic susceptibility M_i/H of this semimetal on the temperature and the magnetic field, Figs. 3–5. In particular, for magnetic fields directed along the z axis, we find that the strong dependence of the chemical potential on the magnetic field noticeably changes the shape of the de Haas-van Alphen oscillations and completely masks their phase shift caused by the Berry phase.

APPENDIX: ELECTRON SPECTRUM IN A MAGNETIC FIELD

Here we justify formulas (2) and (3). If $\theta = 0$, these formulas exactly describe the electron spectrum in the magnetic field [36]. At a nonzero θ, for points of the line, p_c, at which $\varepsilon_d(p_3)$ reaches its minimum ε_{min} or maximum ε_{max} values, i.e., where $\varepsilon_d(p_3)$ can be represented in the form $\varepsilon_d(p_3) \approx \varepsilon_{min} + B(p_3 - p_c)^2$ or $\varepsilon_d(p_3) \approx \varepsilon_{max} - B(p_3 - p_c)^2$ with a positive constant B, formulas (2) and (3) approximately hold in the leading order in the small parameter η^2 [36],

$$\eta^2 = \frac{B|\zeta - \varepsilon_c|\tan^2\theta}{V^2} \ll 1. \tag{A1}$$

Here, $V^2 \sim (b_{11}b_{22})^{1/2}$, ζ is the chemical potential of the electrons in a semimetal, $\varepsilon_c = \varepsilon_{min}$ or ε_{max}, and it is implied in Eq. (A1) that θ is not close to $\pi/2$. Consider now a point of the line, $p_3^{(0)}$, at which $a_3 \equiv d\varepsilon_d(p_3)/dp_3 \neq 0$. At this point

of general position, the spectrum described by Eq. (1) can be formally obtained, setting $b_{33} \to 0$ in the spectrum of the Dirac point:

$$\varepsilon_{c,v} = \varepsilon_d\left(p_3^{(0)}\right) + a_3\delta p_3 + \mathbf{a}_\perp\mathbf{p}_\perp \pm E_{c,v},$$
$$E_{c,v}^2 = b_{11}(p_1)^2 + b_{22}(p_2)^2 + b_{33}(\delta p_3)^2, \qquad \text{(A2)}$$

where $\delta p_3 \equiv p_3 - p_3^{(0)}$. In a magnetic field $\mathbf{H} = \mathbf{n}H$ directed along an arbitrary unit vector $\mathbf{n}$, the exact spectrum of electrons described by Hamiltonian (A2) has the form [5,36]

$$\varepsilon_{c,v}^l(p_n) = \varepsilon_d(p_3^{(0)}) + vp_n \pm \left[\frac{e\hbar\alpha_D H}{c}\, l + L\,(p_n)^2\right]^{1/2}, \qquad \text{(A3)}$$

where $l = 0,1,2,\ldots$; p_n is the component of the quasimomentum along the magnetic field,

$$\alpha_D = \frac{2R_n^{3/2}}{b_{11}b_{22}b_{33}\tilde{\mathbf{n}}^2},$$
$$L = \frac{R_n}{b_{11}b_{22}b_{33}\tilde{\mathbf{n}}^4},$$
$$R_n = b_{11}b_{22}b_{33}(\tilde{\mathbf{n}}^2 - [\tilde{\mathbf{n}}\times\tilde{\mathbf{a}}]^2),$$
$$v = \frac{(\tilde{\mathbf{a}}\tilde{\mathbf{n}})}{\tilde{\mathbf{n}}^2}, \qquad \text{(A4)}$$

and the components of the vectors $\tilde{\mathbf{n}}$ and $\tilde{\mathbf{a}}$ are defined by the relations:

$$\tilde{n}_i \equiv \frac{n_i}{\sqrt{b_{ii}}}, \quad \tilde{a}_i \equiv \frac{a_i}{\sqrt{b_{ii}}}. \qquad \text{(A5)}$$

In the limit $b_{33} \to 0$, we find

$$R_n \approx b_{11}b_{22}\left(n_3^2(1-\tilde{a}_\perp^2) - a_3^2\left(\tilde{n}_1^2+\tilde{n}_2^2\right)\right),$$
$$v \approx \frac{a_3}{n_3},$$
$$\alpha_D \approx 2(b_{11}b_{22})^{1/2}(1-\tilde{a}_\perp^2)^{3/2}n_3\left(1 - \frac{a_3^2\left(\tilde{n}_1^2+\tilde{n}_2^2\right)}{n_3^2(1-\tilde{a}_\perp^2)}\right),$$
$$L \propto b_{33} \to 0, \qquad \text{(A6)}$$

where $n_3 = \cos\theta$. Estimating the ratio $a_3^2(\tilde{n}_1^2+\tilde{n}_2^2)/n_3^2(1-\tilde{a}_\perp^2)$, we obtain

$$\frac{a_3^2\left(\tilde{n}_1^2+\tilde{n}_2^2\right)}{n_3^2(1-\tilde{a}_\perp^2)} \sim \frac{a_3^2\tan^2\theta}{V^2} \sim \frac{\Delta^2\tan^2\theta}{L^2V^2}, \qquad \text{(A7)}$$

where $2\Delta \equiv \varepsilon_{\max} - \varepsilon_{\min}$, and L is the length of the band-contact line in the Brillouin zone. Since Δ is assumed to be small as compared to the characteristic scale $LV \sim 1$ eV of the electron band structure in the line-node semimetals, the above ratio is small, too, and it does not exceed the parameter η^2. Hence $\alpha_D \approx \alpha\cos\theta$, where α is given by Eq. (3). With the relation $vp_n \approx (a_3/\cos\theta)p_n = a_3\delta p_3$, we find that formula (A3) reduces to Eq. (2) for a point $p_3^{(0)}$ of general position.

[1] X. Wan, A. M. Turner, A. Vishwanath, and S. Y. Savrasov, Phys. Rev. B **83**, 205101 (2011).
[2] A. A. Burkov, M. D. Hook, and L. Balents, Phys. Rev. B **84**, 235126 (2011).
[3] S. M. Young, S. Zaheer, J. C. Y. Teo, C. L. Kane, E. J. Mele, and A. M. Rappe, Phys. Rev. Lett. **108**, 140405 (2012).
[4] A. Soluyanov, D. Gresch, Z. Wang, Q. Wu, M. Troyer, X. Dai, and B. A. Bernevig, Nature (London) **527**, 495 (2015).
[5] G. P. Mikitik and Yu. V. Sharlai, Phys. Rev. B **94**, 195123 (2016);
[6] Z. Wang, H. Weng, Q. Wu, X. Dai, and Z. Fang, Phys. Rev. B **88**, 125427 (2013).
[7] M. Neupane, S.-Y. Xu, R. Sankar, N. Alidoust, G. Bian, C. Liu, I. Belopolski, T.-R. Chang, H.-T. Jeng, H. Lin, A. Bansil, F. Chou, and M. Z. Hasan, Nat. Commun. **5**, 3786 (2014).
[8] S. Borisenko, Q. Gibson, D. Evtushinsky, V. Zabolotnyy, B. Büchner, and R. J. Cava, Phys. Rev. Lett. **113**, 027603 (2014).
[9] S. Jeon, B. B. Zhou, A. Gyenis, B. E. Feldman, I. Kimchi, A. C. Potter, Q. Gibson, R. J. Cava, A. Vishwanath, and A. Yazdani, Nat. Mater. **13**, 851 (2014).
[10] T. Liang, Q. Gibson, M. N. Ali, M. Liu, R. J. Cava, and N. P. Ong, Nat. Mater. **14**, 280 (2015).
[11] M. N. Ali, Q. Gibson, S. Jeon, B. B. Zhou, A. Yazdani, and R. J. Cava, Inorg. Chem. **53**, 4062 (2014).
[12] Z. K. Liu, J. Jiang, B. Zhou, Z. J. Wang, H. M. Weng, D. Prabhakaran, S.-K. Mo, H. Peng, P. Dudin, T. Kim, M. Hoesch, Z. Fang, X. Dai, Z. X. Shen, D. L. Feng, Z. Hussain, and Y. L. Chen, Nat. Mater. **13**, 677 (2014).
[13] Z. Wang, Y. Sun, X.-Q. Chen, C. Franchini, G. Xu, H. Weng, X. Dai, and Z. Fang, Phys. Rev. B **85**, 195320 (2012).
[14] Z. K. Liu, B. Zhou, Y. Zhang, Z. J. Wang, H. M. Weng, D. Prabhakaran, S.-K. Mo, Z. X. Shen, Z. Fang, X. Dai, Z. Hussain, and Y. L. Chen, Science **343**, 864 (2014).
[15] H. Weng, C. Fang, Z. Fang, B. A. Bernevig, and X. Dai, Phys. Rev. X **5**, 011029 (2015).
[16] S.-M. Huang, S.-Y. Xu, I. Belopolski, C.-C. Lee, G. Chang, B. Wang, N. Alidoust, G. Bian, M. Neupane, C. Zhang, S. Jia, A. Bansil, H. Lin, and M. Z. Hasan, Nat. Commun. **6**, 7373 (2015).
[17] S.-Y. Xu, I. Belopolski, N. Alidoust, M. Neupane, G. Bian, C. Zhang, R. Sankar, G. Chang, Z. Yuan, C.-C. Lee, S.-M. Huang, H. Zheng, J. Ma, D. S. Sanchez, B. Wang, A. Bansil, F. Chou, P. P. Shibayev, H. Lin, S. Jia, and M. Z. Hasan, Science **349**, 613 (2015).
[18] B. Q. Lv, H. M. Weng, B. B. Fu, X. P. Wang, H. Miao, J. Ma, P. Richard, X. C. Huang, L. X. Zhao, G. F. Chen, Z. Fang, X. Dai, T. Qian, and H. Ding, Phys. Rev. X **5**, 031013 (2015).
[19] C. Shekhar, A. K. Nayak, Y. Sun, M. Schmidt, M. Nicklas, I. Leermakers, U. Zeitler, Y. Skourski, J. Wosnitza, Z. Liu, Y. Chen, W. Schneller, H. Borrmann, Y. Grin, C. Felser, and B. Yan, Nat. Phys. **11**, 645 (2015).
[20] T. T. Heikkilä and G. E. Volovik, JETP Lett. **93**, 59 (2011).
[21] D. Pierucci, H. Sediri, M. Hajlaoui, J.-C. Girard, T. Brumme, M. Calandra, E. Velez-Fort, G. Patriarche, M. G. Silly, G. Ferro, V. Soulière, M. Marangolo, F. Sirotti, F. Mauri, and A. Ouerghi, ACS Nano **9**, 5432 (2015).
[22] H. Weng, Y. Liang, Q. Xu, R. Yu, Z. Fang, X. Dai, and Y. Kawazoe, Phys. Rev. B **92**, 045108 (2015).
[23] K. Mullen, B. Uchoa, and D. T. Glatzhofer, Phys. Rev. Lett. **115**, 026403 (2015).

[24] L. S. Xie, L. M. Schoop, E. M. Seibel, Q. D. Gibson, W. Xie, and R. J. Cava, APL Mater. **3**, 083602 (2015).

[25] Y. Kim, B. J. Wieder, C. L. Kane, and A. M. Rappe, Phys. Rev. Lett. **115**, 036806 (2015).

[26] R. Yu, H. Weng, Z. Fang, X. Dai, and X. Hu, Phys. Rev. Lett. **115**, 036807 (2015).

[27] A. Yamakage, Y. Yamakawa, Y. Tanaka, and Y. Okamoto, J. Phys. Soc. Jpn. **85**, 013708 (2016).

[28] M. Phillips and V. Aji, Phys. Rev. B **90**, 115111 (2014).

[29] L. M. Schoop, M. N. Ali, C. Straßer, V. Duppel, S. S. P. Parkin, B. V. Lotsch, and C. R. Ast, Nat. Commun. **7**, 11696 (2016).

[30] M. Neupane, I. Belopolski, M. M. Hosen, D. S. Sanchez, R. Sankar, M. Szlawska, S.-Y. Xu, K. Dimitri, N. Dhakal, P. Maldonado, P. M. Oppeneer, D. Kaczorowski, F. Chou, M. Z. Hasan, and T. Durakiewicz, Phys. Rev. B **93**, 201104(R) (2016).

[31] A. Topp, J. M. Lippmann, A. Varykhalov, V. Duppel, B. V. Lotsch, C. R. Ast, and L. M. Schoop, New J. Phys. **18**, 125014 (2016).

[32] H. Huang, J. Liu, D. Vanderbilt, and W. Duan, Phys. Rev. B **93**, 201114(R) (2016).

[33] G. Bian, T.-R. Chang, R. Sankar, S.-Y. Xu, H. Zheng, T. Neupert, C.-K. Chiu, S.-M. Huang, G. Chang, I. Belopolski, D. S. Sanchez, M. Neupane, N. Alidoust, C. Liu, B. Wang, C.-C. Lee, H.-T. Jeng, C. Zhang, Z. Yuan, S. Jia, A. Bansil, F. Chou, H. Lin, and M. Z. Hasan, Nat. Commun. **7**, 10556 (2016).

[34] Y. Chen, Y.-M. Lu, and H.-Y. Kee, Nat. Commun. **6**, 6593 (2015).

[35] G. P. Mikitik and I. V. Svechkarev, Fiz. Nizk. Temp. **15**, 295 (1989) [Sov. J. Low Temp. Phys. **15**, 165 (1989)].

[36] G. P. Mikitik and Yu. V. Sharlai, Fiz. Nizk. Temp. **22**, 762 (1996) [Low Temp. Phys. **22**, 585 (1996)].

[37] M. Koshino and T. Ando, Phys. Rev. B **81**, 195431 (2010).

[38] B. Roy and J. D. Sau, Phys. Rev. B **92**, 125141 (2015).

[39] C. Herring, Phys. Rev. **52**, 365 (1937).

[40] G. P. Mikitik, Yu. V. Sharlai, Phys. Rev. B **90**, 155122 (2014).

[41] C. Fang, Y. Chen, H.-Y. Kee, and L. Fu, Phys. Rev. B **92**, 081201(R) (2015).

[42] G. P. Mikitik, Yu. V. Sharlai, Phys. Rev. B **73**, 235112 (2006).

[43] G. P. Mikitik and Yu. V. Sharlai, Fiz. Nizk. Temp. **41**, 1279 (2015) [Low Temp. Phys. **41**, 996 (2015)].

[44] F. Szmulowicz, Solid State Commun. **148**, 410 (2008).

[45] G. P. Mikitik and Yu. V. Sharlai, Phys. Rev. Lett. **93**, 106403 (2004).

[46] M. Koshino and I. F. Hizbullah, Phys. Rev. B **93**, 045201 (2016).

[47] J. W. McClure, Carbon **7**, 425 (1969).

[48] N. B. Kopnin and T. T. Heikkilä, Surface Superconductivity in Rhombohedral Graphite, Ch. 9 in *Carbon-based Superconductors: Towards High-Tc Superconductivity*, edited by J. Haruyama (Pan Stanford, 2014), see also arXiv:1210.7075.

[49] If $\tilde{a}_\perp^2 > 1$ for a part of the band-contact line, this part should be disregarded in all subsequent formulas.

[50] In formula (10) of Ref. [5], the numerical coefficient should be 0.11×10^{12} rather than 0.7×10^{12}. This correction leads to $H_T \sim 2 - 200$ Oe at $T = 4$ K instead of the estimate $H_T \sim$ 10–1000 Oe given in Ref. [5].

[51] See Supplemental Material at http://link.aps.org/supplemental/10.1103/PhysRevB.97.085122 for the derivation of the expressions for the Ω potential and the magnetization.

[52] Yu. B. Rumer and M. Sh. Ryvkin, *Thermodynamics, Statistical Physics, and Kinetics* (Mir, Moscow, 1980).

[53] M. Koshino and T. Ando, Phys. Rev. B **75**, 235333 (2007).

[54] S. G. Sharapov, V. P. Gusynin, and H. Beck, Phys. Rev. B **69**, 075104 (2004).

[55] D. Shoenberg, *Magnetic Oscillations in Metals* (Cambridge University Press, Cambridge, England, 1984).

[56] G. P. Mikitik and Yu. V. Sharlai, Fiz. Nizk. Temp. **33**, 586 (2007) [Low Temp. Phys. **33**, 439 (2007)].

[57] G. P. Mikitik, Yu. V. Sharlai, Phys. Rev. Lett. **82**, 2147 (1999).

[58] G. P. Mikitik and Yu. V. Sharlai, Zh. Eksp. Teor. Fiz. **114**, 1375 (1998) [J. Exp. Theor. Phys. **87**, 747 (1998)].

[59] G. P. Mikitik and Yu. V. Sharlai, Phys. Rev. B **65**, 184426 (2002).

[60] M. N. Ali, L. M. Schoop, C. Garg, J. M. Lippmann, E. Lara, B. Lotsch, and S. S. P. Parkin, Sci. Adv. **2**, e1601742 (2016).

[61] X. Wang, X. Pan, M. Gao, J. Yu, J. Jiang, J. Zhang, H. Zuo, M. Zhang, Z. Wei, W. Niu, Z. Xia, X. Wan, Y. Chen, F. Song, Y. Xu, B. Wang, G. Wang, and R. Zhang, Adv. Electron. Mater. **2**, 1600228 (2016).

[62] J. Hu, Z. Tang, J. Liu, Y. Zhu, J. Wei, and Z. Mao, Phys. Rev. B **96**, 045127 (2017).

[63] S. Pezzini, M. R. van Delft, L. M. Schoop, B. V. Lotsch, A. Carrington, M. I. Katsnelson, N. E. Hussey, and S. Wiedmann, Nat. Phys. **14**, 178 (2018).

[64] R. Singha, A. K. Pariari, B. Satpati, and P. Mandal, Proc. Natl. Acad. Sci. USA **114**, 2468 (2017).

[65] M. Matusiak, J. R. Cooper, and D. Kaczorowski, Nat. Commun. **8**, 15219 (2017).

[66] J. Hu, Z. Tang, J. Liu, X. Liu, Y. Zhu, D. Graf, K. Myhro, S. Tran, C. N. Lau, J. Wei, and Z. Mao, Phys. Rev. Lett. **117**, 016602 (2016).

[67] K. S. Novoselov, A. K. Geim, S. V. Morozov, D. Jiang, M. I. Katsnelson, I. V. Grigorieva, S. V. Dubonos, and A. A. Firsov, Nature (London) **438**, 197 (2005).

[68] Y. Zhang, Y.-W. Tan, H. L. Stormer, and P. Kim, Nature (London) **438**, 201 (2005).

[69] G. P. Mikitik and Yu. V. Sharlai, Fiz. Nizk. Temp. **43**, 200 (2017) [Low Temp. Phys. **43**, 168 (2017)].